Construction and evolution of an *Escherichia coli* strain relying on nonoxidative glycolysis for sugar catabolism

Paul P. Lin[a,1], Alec J. Jaeger[a,1], Tung-Yun Wu[a], Sharon C. Xu[a], Abraxa S. Lee[a], Fanke Gao[a], Po-Wei Chen[a], and James C. Liao[b,2]

[a]Department of Chemical and Biomolecular Engineering, University of California, Los Angeles, CA 90095; and [b]Institute of Biological Chemistry, Academia Sinica, 115 Taipei, Taiwan

This contribution is part of the special series of Inaugural Articles by members of the National Academy of Sciences elected in 2015.

Contributed by James C. Liao, February 23, 2018 (sent for review February 6, 2018; reviewed by Ramon Gonzalez and Eleftherios Papoutsakis)

The Embden–Meyerhoff–Parnas (EMP) pathway, commonly known as glycolysis, represents the fundamental biochemical infrastructure for sugar catabolism in almost all organisms, as it provides key components for biosynthesis, energy metabolism, and global regulation. EMP-based metabolism synthesizes three-carbon (C3) metabolites before two-carbon (C2) metabolites and must emit one CO_2 in the synthesis of the C2 building block, acetyl-CoA, a precursor for many industrially important products. Using rational design, genome editing, and evolution, here we replaced the native glycolytic pathways in *Escherichia coli* with the previously designed nonoxidative glycolysis (NOG), which bypasses initial C3 formation and directly generates stoichiometric amounts of C2 metabolites. The resulting strain, which contains 11 gene overexpressions, 10 gene deletions by design, and more than 50 genomic mutations (including 3 global regulators) through evolution, grows aerobically in glucose minimal medium but can ferment anaerobically to products with nearly complete carbon conservation. We confirmed that the strain metabolizes glucose through NOG by ^{13}C tracer experiments. This redesigned *E. coli* strain represents a different approach for carbon catabolism and may serve as a useful platform for bioproduction.

Escherichia coli | evolution | glycolysis | metabolic engineering | synthetic biology

The Embden–Meyerhoff–Parnas (EMP) pathway provides the fundamental structure for carbon metabolism in almost all living organisms. A variety of carbon sources are metabolized through this pathway to synthesize three-carbon (C3; e.g., pyruvate) and two-carbon (C2; e.g., acetyl-CoA) metabolites, which are precursors in almost all biosynthetic and energy metabolism pathways. Acetyl-CoA is also an important metabolic precursor to a variety of industrially relevant compounds, including fatty acids, alcohols, alkanes, isoprenoids, and polyketides (1, 2). Acetyl-CoA is typically produced via decarboxylation of pyruvate. Thus, a key limitation for producing acetyl-CoA–derived bioproducts is the intrinsic carbon loss in acetyl-CoA biosynthesis. Pyruvate decarboxylation releases the carboxyl group of pyruvate as carbon dioxide or formate to the environment. Therefore, the maximum carbon yield of acetyl-CoA–derived products would be capped to only 67% unless carbon dioxide or formate is reassimilated through carbon fixation pathways. *Bifidobacteria* use a "bifido shunt" to partially bypass pyruvate and improve carbon yield (3), and expression of phosphoketolase (Xpk) has been shown to increase the production of acetyl-CoA–derived products (4–6). However, these organisms still largely rely on the EMP and the pentose phosphate pathway for sugar catabolism.

Recently, Bogorad et al. (7) designed a synthetic pathway termed nonoxidative glycolysis (NOG), which uses Xpk-dependent cleavage of sugar phosphates and carbon rearrangement cycles to generate acetyl-CoA with complete carbon conservation. An engineered *Escherichia coli* strain, JCL118, was able to convert 88% of pentose carbon to acetate with the expression of NOG. This provides a proof of concept and a significant improvement over the theoretical maximum of 67%. Although the biochemical path of NOG was shown in this strain, the NOG cycle alone cannot support growth in minimal medium with sugar as the sole carbon source unless native glycolytic pathways are also partially used to generate pyruvate and other essential biosynthetic precursors. This situation significantly limits the utility of this strain. Furthermore, the NOG cycle must be able to catabolize sugar at a reasonable rate while being robust.

To overcome the above challenges, here we design and evolve an *E. coli* strain that relies on NOG for carbon catabolism to support growth. All of the native pathways for sugar metabolism are blocked by gene deletions, and the cells are forced to use NOG to synthesize acetyl-CoA. We then use TCA cycle, glyoxylate shunt (GS), and gluconeogenesis to convert acetyl-CoA to all required components (e.g., pyruvate) to allow for growth in glucose minimal medium. The cells derive reducing equivalents and ATP through the TCA cycle and respiration and thus, can grow in glucose minimal medium only under aerobic conditions. After growth, the cells metabolize glucose through NOG to produce acetate at a nearly 100% carbon yield under anaerobic or fermentation conditions. This strategy allows for a clear separation between the growth and production phases. Furthermore, coupling NOG with growth enables the tuning of metabolic networks

Significance

We constructed an *Escherichia coli* strain that does not use glycolysis for sugar catabolism. Instead, it uses the synthetic nonoxidative glycolysis cycle to directly synthesize stoichiometric amounts of the two-carbon building block (acetyl-CoA), which is then converted to three-carbon metabolites to support growth. The resulting strain grows aerobically in glucose minimal medium and can achieve near-complete carbon conservation in the production of acetyl-CoA–derived products during anaerobic fermentation. This strain improves the theoretical carbon yield from 66.7% to 100% in acetyl-CoA–derived product formation.

Author contributions: P.P.L., A.J.J., T.-Y.W., P.-W.C., and J.C.L. designed research; P.P.L., A.J.J., T.-Y.W., S.C.X., A.S.L., F.G., and P.-W.C. performed research; P.P.L., A.J.J., T.-Y.W., and P.-W.C. analyzed data; and P.P.L., A.J.J., and J.C.L. wrote the paper.

Reviewers: R.G., Rice University; and E.P., University of Delaware.

The authors declare no conflict of interest.

Data deposition: The NOG21 sequence reported in this paper has been deposited in the Sequence Read Archive (accession no. SRP133030).

[1]P.P.L. and A.J.J. contributed equally to this work.

[2]To whom correspondence should be addressed. Email: liaoj@gate.sinica.edu.tw.

This article contains supporting information online at www.pnas.org/lookup/suppl/doi:10.1073/pnas.1802191115/-/DCSupplemental.

Published online March 19, 2018.

and global regulatory circuits through directed strain evolution to adapt to the biochemical infrastructure.

Results

Rationale of Strain Design. The overall reactions to synthesize pyruvate and acetyl-CoA using EMP-based metabolism are

$$\text{Glucose} \rightarrow 2 \text{ pyruvate} + 2 \text{ NADH} + 2 \text{ ATP}$$

$$\text{Glucose} \rightarrow 2 \text{ acetyl-CoA} + 2 \text{ CO}_2 + 4 \text{ NADH} + 2 \text{ ATP}.$$

These reactions not only provide crucial biosynthetic precursors but also partially oxidize glucose to derive reducing equivalents and ATP for growth and maintenance. The distributions of the C3 and C2 metabolites as well as reducing equivalents and ATP are presumably optimized for various cellular functions. When NOG is used to metabolize glucose, it requires an ATP to phosphorylate the carbohydrate and forms three acetyl-CoA per glucose:

$$\text{Glucose} + \text{ATP} \rightarrow 3 \text{ acetyl CoA}.$$

ATP can be provided by converting acetyl-CoA to acetate:

$$\text{Glucose} \rightarrow 2 \text{ acetyl-CoA} + \text{acetate}.$$

Thus, NOG is more efficient in retaining C-C bounds and does not generate CO_2, but it does not produce reducing equivalents for biosynthesis. Since CO_2 fixation is a major challenge for most microbes, it is useful to retain carbon during fermentation. Furthermore, because of the fast development and deployment of renewable electricity, external reducing equivalents, such as renewable hydrogen or formic acid, are expected to become available and affordable for fermentation processes. These reducing equivalents can then be supplied to the NOG strains to produce products more reduced than acetate.

However, NOG does not provide essential C3 metabolites, and alone, it cannot support growth in glucose minimal medium. Therefore, we planned to connect the NOG pathway with GS and gluconeogenesis to synthesize pyruvate from acetyl-CoA (Fig. 1). In this scheme, acetyl-CoA enters GS to synthesize C4 metabolites, malate, and oxaloacetate (OAA), which are then converted to pyruvate or phosphoenolpyruvate (PEP) through the malic enzymes or phosphoenolpyruvate carboxykinase (Pck). The net reaction for pyruvate synthesis using this scheme is

$$\text{Glucose} + \text{ATP} \rightarrow 1.5 \text{ pyruvate} + 1.5 \text{ CO}_2 + 3 \text{ NADH} + 1.5\text{FADH}_2/\text{quinol}.$$

Under aerobic conditions, ATP is synthesized through respiration. In contrast to the EMP pathway, this NOG-based scheme is less carbon efficient in generating pyruvate, but it is more carbon efficient in synthesizing acetyl-CoA and acetate.

We hypothesized that the NOG-based metabolism can support cell growth in glucose minimal medium only aerobically and produce acetate anaerobically without carbon loss to CO_2. Thus, the growth and production phases can be separated. Our strategy for achieving this design combines rational genetic manipulation and evolution using serial transfer in selective media (Fig. 2). To accelerate evolution, we at times used a separate plasmid (pPL71 in *SI Appendix*, Table S7) to express the mutD5 gene, and its expression has been shown to increase the mutation rate in *E. coli* 37,000-fold in rich medium and 480-fold in minimal medium (8).

Blocking Native Glycolytic Pathways. We first blocked the EMP pathway by deleting the glyceraldehyde-3-phosphate dehydrogenase (*gapA*) gene (step 1 in Fig. 2), which codes for glyceraldehyde 3-phosphate (G3P) dehydrogenase. Deletion of *gapA* abolished growth in glucose minimal medium (9, 10). We also deleted *mgsA*, which codes for methylglyoxal synthase (11), to eliminate a potential bypass that can provide pyruvate from G3P (Fig. 1). The double-deletion strain, PHL2 (Δ*gapA*Δ*msgA*), needs multiple carbon sources to supply essential metabolites upstream or downstream of GapA, such as glycerol and succinate (9).

We then expressed *xpk*, as Xpk is the only enzyme that does not exist in *E. coli*. We cloned *xpk* from *Bifidobacterium adolescentis* under the $P_L lacO_1$ promoter (step 2 in Fig. 2) to construct plasmid pPL157 (*SI Appendix*, Table S7). Since Xpk produces acetyl-CoA, it can theoretically rescue the growth phenotype of the Δ*gapA* strain, even without the complete NOG cycle. However, PHL2/pPL157 failed to grow in glucose minimal medium, suggesting that some of the genes in the desired pathway were insufficiently expressed or that the enzymes were regulated.

We then evolved the strain by serial dilutions in culture tubes containing glucose minimal medium with a limited amount of succinate-glycerol-casamino acid (SGC) mix. SGC was supplied to allow for only limited growth ($OD_{600} < 0.3$). Growth beyond this level indicates the successful utilization of glucose. We evolved PHL2/pPL157 with and without the *mutD5* mutator gene expressed. After 2 mo of evolution without *mutD5*, we could not isolate any mutant capable of growth in minimal medium with glucose as the sole carbon source (step 4a in Fig. 2). However, the same strain with *mutD5* expressed did evolve to grow in glucose minimal medium after 2 wk. Unfortunately, the evolved strain retained the ability to grow in glucose minimal medium after removing the plasmid containing *xpk*, suggesting that this growth phenotype was likely due to pathways independent of NOG (Fig. 2, step 5).

To avoid possible suppressor mutations that restore the carbon flux to pyruvate, we deleted erythrose-4-phosphate dehydrogenase (*gapB*), which codes for a potential GapA isozyme, erythrose 4-phosphate dehydrogenase (12). Another essential EMP gene phosphoglycerate kinase (*pgk*) (10), coding for phosphoglycerate kinase, was also deleted. Furthermore, we deleted the Entner–Dodorouff pathway genes [glucose 6-phosphate dehydrogenase (*zwf*), phosphogluconate dehydratase (*edd*), Entner–Doudoroff aldolase (*eda*)], which can also metabolize glucose to pyruvate. The resulting strain (Δ*gapA*Δ*mgsA*Δ*gapB*Δ*pgk*Δ*zwf*Δ*edd*Δ*eda*) was named PHL7 (step 6 in Fig. 2). We then used the same evolution scheme to evolve PHL7 (step 7 in Fig. 2). The additional gene deletions successfully eliminated possible suppressor mutations that might create alternative pathways, as PHL7 failed to grow in glucose minimal medium after 2 mo of evolution, even with *mutD5*. Therefore, this strain (PHL7) was used as a baseline strain for additional engineering and evolution.

Removing Native Control and Potential Futile Cycles. Since our designed pathway involves a major rewiring of metabolic flux, some of the pathway genes are repressed by native regulators, and futile cycles may exist between the native and rewired pathways. Although these problems in principle could be solved by evolution, we edited the genome to avoid these problems. First, we deleted *iclR*, which codes for a transcriptional repressor (13) that binds to the promoter region of the *aceBAK* operon and controls the GS expression. Second, to up-regulate gluconeogenesis for converting the TCA cycle intermediate OAA to PEP, we replaced the native *pckA* promoter with the $P_L lacO_1$ promoter to eliminate endogenous regulation (14, 15). Furthermore, we deleted two potential futile cycles. The first is between the NOG enzyme fructose bisphosphatase (Fbp) and the glycolytic

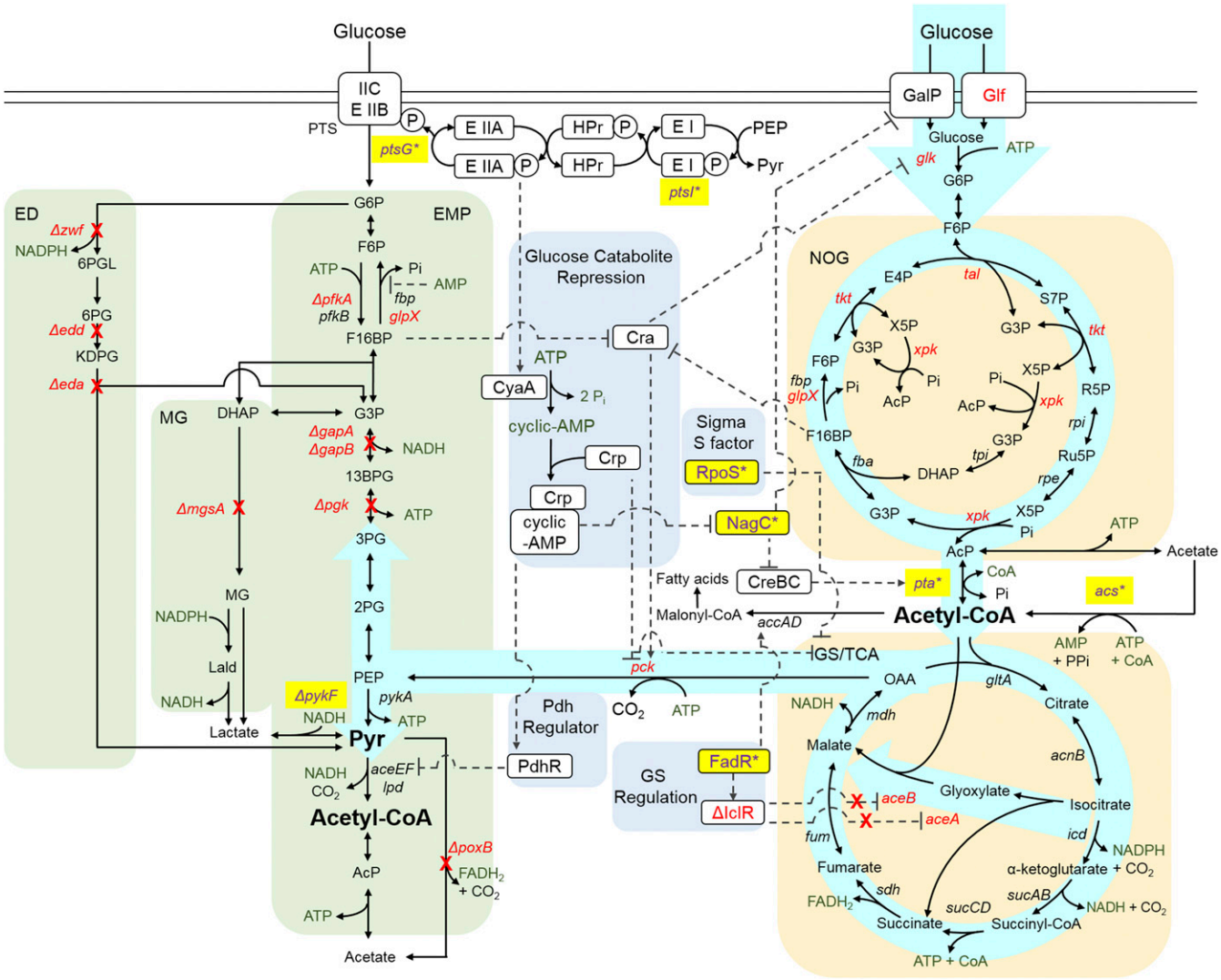

Fig. 1. Metabolic networks in the synthetic *E. coli* NOG strain. The red letters and crosses represent genes overexpressed or deleted. The dashed lines represent regulation. The purple letters highlighted in yellow represent gene mutations through evolution. The cyan highlighted path indicates the general direction of the designed flux during growth. *accAD*, acetyl-CoA carboxyltransferase subunit α and β; *aceA*, isocitrate lyase; *aceB*, malate synthase; *aceEF*, pyruvate dehydrogenase subunits; *acnB*, aconitate hydratase; *acs*, acetyl-CoA synthase; 13BPG, 1,3-bisphosphoglycerate; Cra, catabolite repressor activator; CreBC, a two-component system that responds to growth in minimal medium; Crp, cAMP receptor protein; *cyaA*, adenylate cyclase; DHAP, dihydroxyacetone phosphate; E4P, erythrose 4-phosphate; ED, Entner–Doudoroff; F16BP, fructose 1,6-bisphosphate; FadR, fatty acid metabolism regulator protein; *fba*, F16BP aldolase; *fbp*, fructose 1,6-bisphosphatase; *fum*, fumarase; G6P, glucose 6-phosphate; GalP, galactose:H^+ transporter; *glpX*, type II fructose 1,6-bisphosphatase; *icd*, isocitrate dehydrogenase; IclR, DNA-binding transcriptional repressor for glyoxylate shunt; KDPG, 2-keto-3-deoxy-6-phospho-gluconate; Lald, lactaldehyde; *lpd*, lipoamide dehydrogenase; MG, methylglyoxal; *mgsA*, methylglyoxal synthase; NagC, a DNA-binding transcriptional dual regulator; PdhR, pyruvate dehydrogenase complex regulator; 2PG, 2-phosphoglycerate; 3PG, 3-phosphoglycerate; 6PG, gluconate 6-phosphate; 6PGL, 6-phospho D-glucono-1,5-lactone; *pta*, phosphate acetyltransferase; *ptsG*, glucose-specific phosphotransferase system enzyme IIBC component; *pyk*, pyruvate kinase; Pyr, pyruvate; R5P, ribose 5-phosphate; *rpe*, ribulose-5-phosphate epimerase; *rpi*, ribose-5-phosphate isomerase; RpoS, sigma factor S; Ru5P, ribulose-5-phosphate; S7P, sedoheptulose 7-phosphate; *sdh*, succinate:quinone oxidoreductase; *tpi*, triose phosphate isomerase; X5P, xylulose 5-phosphate.

enzyme phosphofructokinase (Pfk). Thus, we deleted *pfkA*, which is responsible for 90% of the Pfk activity in *E. coli* (16). The other potential futile cycle involves the interconversion between pyruvate and C2 metabolites. The designed NOG strain converts two acetyl-CoA to one pyruvate. Meanwhile, pyruvate oxidase (PoxB) converts pyruvate to acetate with the production of CO_2, thus forming a potential futile cycle that wastes one acetyl-CoA per turn. Hence, we deleted *poxB* to eliminate this possibility. Finally, instead of the plasmid-based expression, we integrated a copy of *xpk* driven by the $P_L lacO_1$ promoter onto the genome to stabilize the phenotype during evolution. These manipulations resulted in PHL13. We verified that these edits increased the activity of isocitrate lyase (*SI Appendix*, Fig. S1*A*), Xpk (*SI Appendix*, Fig. S1*B*), and Pck (*SI Appendix*, Fig. S1*C*) in the lysates relative to its parental strain, JCL16.

Converting Acetyl-CoA to Pyruvate. We then evolved PHL13 for the desired phenotype: growth in glucose minimal medium using NOG. PHL13 was cultured in minimal medium with 10 g/L of glucose and 5 mM acetate (Fig. 2, step 14). Glucose and acetate were expected to provide metabolites upstream and downstream of GapA, respectively, providing a better representation of our designed pathway. (*SI Appendix*, Fig. S2*A*). We planned to wean the strain off acetate until it could grow on glucose alone. Initially, the strain grew slowly in this medium (*SI Appendix*, Fig. S3*A*). After repeated dilutions in liquid medium, the culture

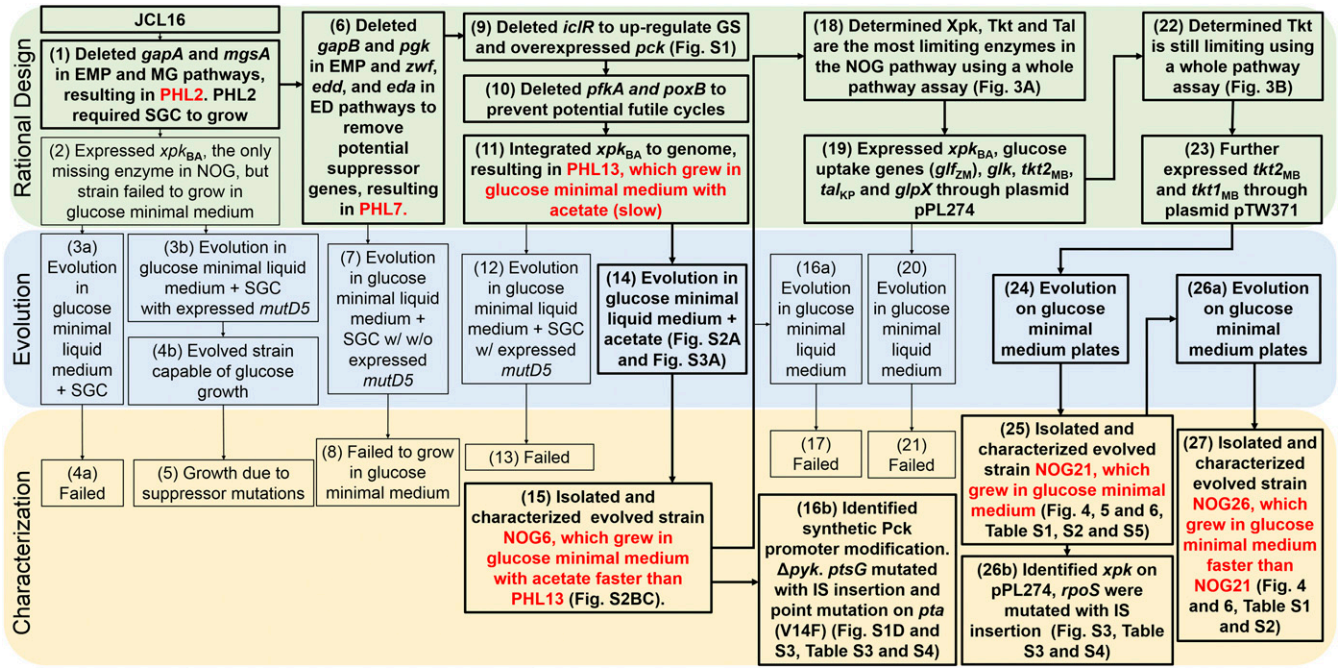

Fig. 2. The flowchart for constructing the synthetic *E. coli* NOG strain. The bold lines represent the successful steps. Enzyme abbreviations are in Fig. 1. SGC is the M9 minimal salt medium with 50 mM glycerol, 50 mM succinate, and 0.1% casamino acid. The subscripts represent the source of the gene: BA, *B. adolescents*; KP, *K. pneumonia*; MB, *M. buryatense* 5GB1; ZM, *Z. mobilis*. Gene locus number: *tkt1*, WP_017840137; *tkt2*, WP_017841573.

evolved to grow reliably in the combination of glucose and acetate. At this time, a single colony (NOG6) that was able to grow the best on the combination of glucose and acetate (*SI Appendix*, Fig. S2 *B* and *C*) was isolated (Fig. 2, step 15). This strain primarily consumed acetate, and its final OD was dependent on the amount of acetate supplied (*SI Appendix*, Fig. S2*C*). While the conversion from glucose to acetyl-CoA was not sufficient to support growth, NOG6 had an improved ability to turn C2 metabolites into biosynthetic precursors under glucose condition.

After isolating NOG6, we continued to evolve this strain in glucose minimal medium with decreasing amounts of acetate (Fig. 2, step 16a). Although we were able to improve the growth rate on the combination of glucose and acetate, we were unable to eliminate acetate in the medium or improve the maximum cell density on glucose and acetate by serial dilutions.

Identifying Limiting Steps in NOG and Achieving Growth on Glucose. To identify limiting enzymes in the NOG cycle for the production of C2 metabolites, we devised a whole-pathway assay using augmented crude extract (Fig. 2, step 18). In these assays, fructose 6-phosphate (F6P) was used as the initial substrate, and acetyl phosphate (AcP) production was measured colorimetrically (7). As a positive control, a mixture containing all eight purified enzymes involved in NOG was added to the crude extract of NOG6. We then determined the effect of removing a particular enzyme in the purified enzyme mixture. The extent to which removal of an enzyme lowers the AcP production compared with the positive control indicates its deficiency in the strain, as enzymes with large drop-offs after their removal are likely not expressed sufficiently. Performing this assay on NOG6, we identified Xpk as a possible limiting enzyme followed by transketolase (Tkt) and transladolase (Tal) (Fig. 3*A*). Since Xpk has a much higher specific activity for xylulose 5-phosphate (3.5 μmol/min per milligram protein) than F6P (0.71 μmol/min per milligram protein) (7), which was not tested in this experiment, the limiting strength of this enzyme is less certain. Nevertheless, these enzymes were to be augmented using plasmid expression.

Other than the limiting enzymes identified from the whole-pathway assay, there were two additional factors that could be hindering growth: (*i*) inefficient glucose transport and (*ii*) allosteric regulation of the NOG pathway enzymes. Wild-type *E. coli* uses the phosphotransferase system (PTS) for glucose transport, which requires PEP as the phosphoryl group donor. Since the designed NOG strain does not synthesize PEP directly, it may benefit from a glucose transport system independent of PTS. We thus expressed the *Zymomonas mobilis* glucose facilitator (*glf*) (17) gene in NOG6. We also overexpressed the native glucokinase (*glk*), since it has been reported that growth on glucose reduced the *glk* expression by 50% (18). Moreover, since *E. coli* Fbp is inhibited by AMP (19) and glucose 6-phosphate (20), we overexpressed *glpX*, which codes for an isozyme of Fbp independent of AMP regulation. Together, the plasmid pPL274 was constructed to express *xpk*, *glf*, *glk*, *tkt2* (WP_017841573 from *Methylomicrobium buryatense 5GB1*), *tal* (from *Klebsiella pneumoniae*), and *glpX* and was transformed into NOG6 (Fig. 2, step 19). *M. buryatense 5GB1 tkt2* (WP_017841573) and *K. pneumonia tal* were chosen over the *E. coli tkt* and *tal* because of their better activity at low ribose 5-phosphate concentrations (*SI Appendix*, Fig. S4) based on in vitro assays using purified enzymes.

We applied the same evolution scheme to evolve NOG6/pPL274 (steps 20 and 21 in Fig. 2). Unfortunately, NOG6/pPL274 still did not develop a growth phenotype in glucose minimal liquid medium after 2 mo of evolution without *mutD5* expression. We repeated the whole-pathway assay and identified that Tkt was the most limiting in the crude extract of NOG6/pPL274 (Fig. 3*B*). Therefore, we transformed the NOG6/pPL274 strain with an additional plasmid (pTW371) for expressing two *tkt* genes (WP_017841573 and WP_017840137) from *M. buryatense 5GB1*. Finally, the strain NOG6/pPL274/pTW371 was able to grow (from OD_{600} = 0.1–0.8) in minimal liquid medium with glucose as the sole carbon source after 8 d. We further improved the growth rate by the serial streaking of colonies on glucose minimal medium

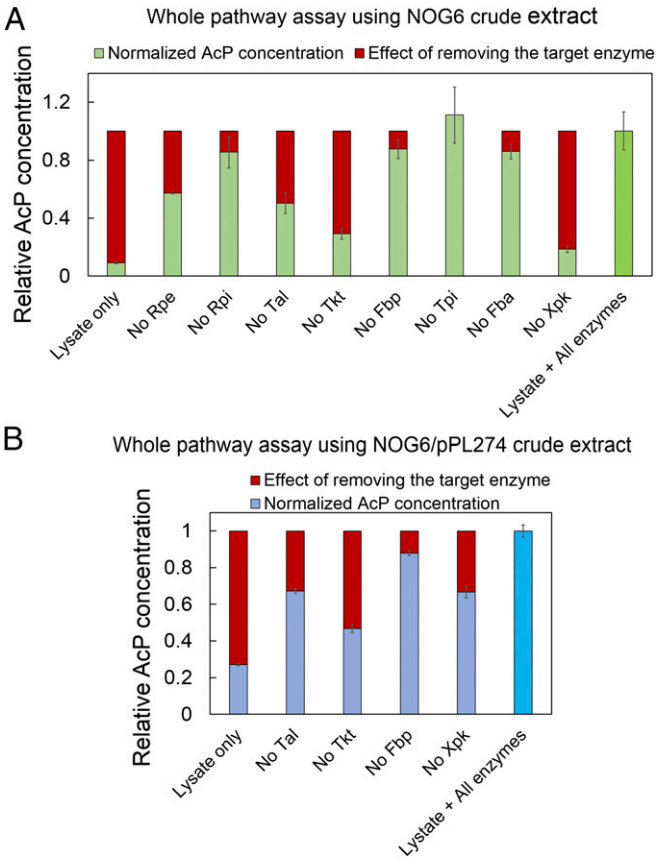

Fig. 3. Identification of limiting enzymes in the NOG pathway through a whole-pathway assay using strain lysates. (*A*) Whole-pathway assay on NOG6 lysate shows that Xpk is likely the most limiting enzyme for AcP production followed by Tkt and Tal. (*B*) Whole-pathway assay on NOG6/pPL274 lysate shows that Tkt is the most limiting enzyme. Enzyme abbreviations are in Fig. 1. Plasmid pPL274 contains xpk_{BA}, glf_{ZM}, *glk*, $tkt2_{MB}$, tal_{KP}, and *glpX* driven by the $P_L lacO_1$ promoter. Error bars represent the SD ($n = 3$). BA, *B. adolescents*; KP, *K. pneumonia*; MB, *M. buryatense* 5GB1; ZM, *Z. mobilis*.

plates for 1 mo. A fast-growing colony, NOG21, was isolated (Fig. 2, step 25). We continued to evolve NOG21 for another month and isolated NOG26.

Growth Characterization of the NOG Strains. To examine whether the growth of these NOG strains depended on the designed pathway, we removed both plasmids (pPL274*, which acquired a transposon insertion at the 177 nucleotide of Xpk during evolution, and pTW371) from NOG21 and NOG26 to form NOG22 and NOG27, respectively. NOG22 did not grow in glucose minimal medium, and NOG27 barely grew (Fig. 4*A*). We further deleted *xpk* from the NOG27 genome and retransformed it with pPL274* and pTW371 to create NOG28. NOG28 completely lost the growth phenotype in glucose minimal medium under aerobic conditions (Fig. 4*A*). These results indicated that the integrated *xpk* was essential and that the genes harbored on pPL274* and pTW371 were beneficial for the NOG strains.

The doubling times of NOG21 and NOG26 were about 4.8 and 3.6 h, respectively, in glucose minimal medium under aerobic conditions (Fig. 4*B*), which were slower than that of the wild-type strain (JCL16) (doubling time 1.8 h in Fig. 4*B* and *SI Appendix*, Table S1). This result is expected, as the NOG-based metabolic scheme was not predicted to be beneficial to growth, although it is more carbon efficient for C2 synthesis.

However, NOG21 and NOG26 grew at a similar rate compared with JCL16 in LB media and LB plus glucose under aerobic conditions (Fig. 4*B* and *SI Appendix*, Table S2), indicating that the NOG strains were generally healthy. As predicted, NOG21 and NOG26 did not grow under anaerobic conditions in glucose minimal medium (Fig. 4*B* and *SI Appendix*, Tables S1 and S2).

Genome Characterization of the NOG Strains. To understand the genomic changes during evolution, we sequenced PHL13, NOG6, and NOG21 (*SI Appendix*, Tables S3 and S4). Other than the edited areas, the PHL13 genome was largely the same as the parental wild-type strain JCL16 (*SI Appendix*, Tables S3 and S4). PHL13 grew slowly ($OD_{600} = 0.1–0.3$ in 7 d) in minimal medium with glucose and acetate as the carbon sources. NOG6 was evolved from PHL13 and has improved growth in glucose and acetate minimal medium. Compared with PHL13, NOG6 has 26 transposon insertions (inactivating 22 genes) and two point mutations within protein coding regions and resulting in amino acid substitutions [Pta (V14F) and PtsI (A376T)]. Moreover, there was one missense mutation [formyl-CoA transferase (184_185insG)], one 26-kb truncation (from 1,747,769 to 1,773,895), and a 23-bp deletion within the *pck* synthetic promoter region (*SI Appendix*, Fig. S2*D*). Notably, we found a transposon insertion in *ptsG* (enzyme IIBC of the glucose-specific PTS) at the 450 nucleotide and a point mutation (A376T) in *ptsI* (enzyme I of PTS). PtsG and PtsI are also indirectly involved in glucose catabolite repression (Fig. 1). It has been reported that the level of cAMP was higher in a Δ*ptsG* strain than the wild-type *E. coli* (21). Indeed, the intracellular and extracellular concentrations of cAMP in NOG6 were increased (*SI Appendix*, Fig. S3 *B* and *C*) compared with its parental strain PHL13, suggesting that the carbon regulation of NOG6 is altered significantly. Presumably, the point mutation in *ptsI* did not negatively affect its function.

The higher cAMP concentration likely leads to the activation of catabolic genes, such as *pdhR*, which transcriptionally repress the *pdhR–aceEF–lpd* operon (22); *aceEF* and *lpd* encode the pyruvate dehydrogenase complex, which coverts pyruvate to acetyl-CoA and NADH, losing CO_2. Activation of *pdhR* might help NOG6 to prevent this potential carbon loss. Meanwhile, the high cAMP receptor protein–cAMP concentration should decrease the catabolite repression. As expected (23), the transcriptional levels of *pdhR*, *fumA*, and *sdhA* were increased in NOG6 compared with PHL13 (*SI Appendix*, Fig. S3*D*) by RT-PCR. However, citrate synthase (*gltA*) and malate dehydrogenase (*mdh*) transcriptional levels were roughly the same in both strains.

NOG21 was evolved from NOG6 after being transformed with plasmids pPL274 and pTW371 and can grow in minimal medium with glucose as the sole carbon source. Compared with NOG6, there were an additional 26 transposon insertions, resulting in 16 genes being inactivated. (*SI Appendix*, Table S3). There were also three point mutations within protein coding regions [*yciG* (N35K), *sad* (C423R), and *dfp* (T21N)] and three synonymous amino acid mutations (*SI Appendix*, Table S4). Finally, there were three Indel mutations and four genome truncations (*SI Appendix*, Table S4). Most notably, the *xpk* gene on pPL274 was inactivated by a transposon insertion, and the resulting plasmid is named pPL274*. Although Xpk is the key enzyme in NOG, excessive Xpk activity may drain F6P, leaving no substrate for Tal and causing erythrose 4-phosphate accumulation. This kinetic trap had been identified previously using Ensemble Modeling for Robustness Analysis (EMRA) (24), and evolution likely tuned the activity to the working range.

We also found that *rpoS* (encoding sigma factor S) was mutated by a transposon insertion (at the 832 nucleotide; total size 993 bp). It has been reported that RpoS down-regulates the GS and TCA genes and up-regulates *tktB*, *talA*, and *pfkB* (encoding 6-phosphofructokinase II) during the exponential phase in glucose minimal medium (25). Thus, we measured the transcriptional level of several genes regulated by RpoS, including *tktAB*, *talAB*, *aceAB*,

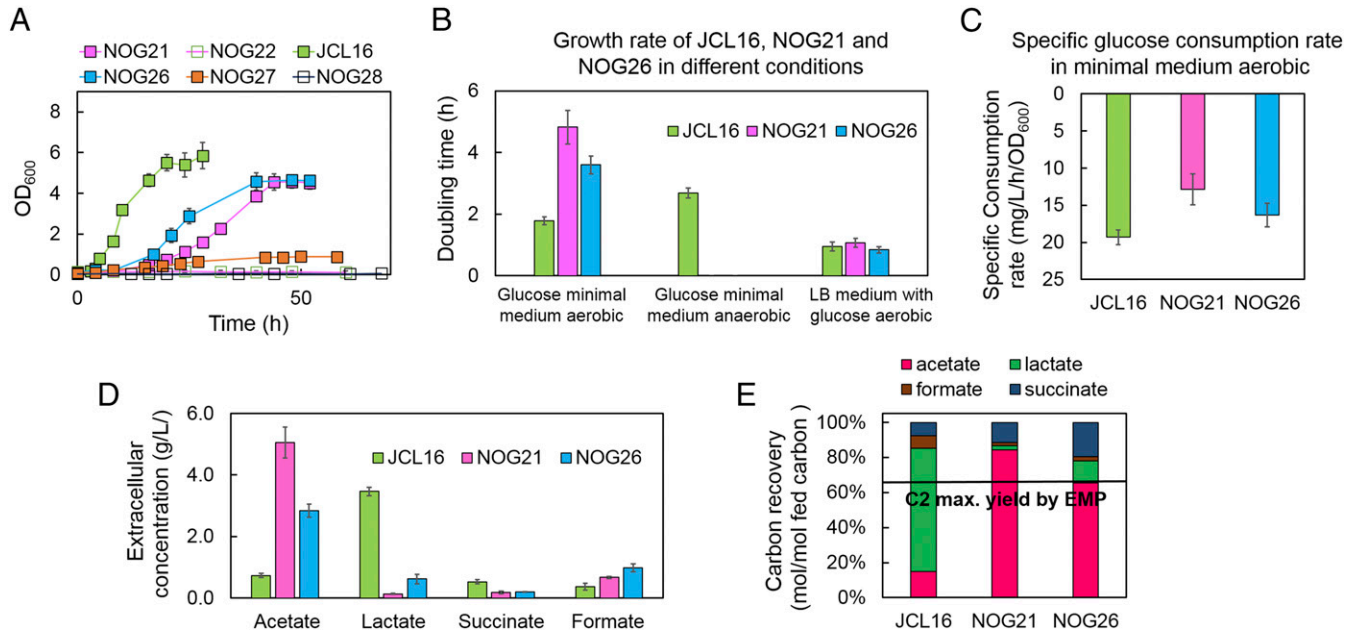

Fig. 4. Growth characterization and anaerobic production of JCL16, NOG21, and NOG26. (*A*) The growth curve of the NOG strains and wild-type *E. coli* (JCL16) in glucose (10 g/L) minimal medium. NOG21 and NOG26 contain two plasmids: pPL274* and pTW371. NOG22 and NOG27 are NOG21 and NOG26 cured of both plasmids. NOG28 is NOG27 with the chromosomal *xpk* deleted and pPL274* and pTW371 retransformed. (*B*) The doubling time of growth in glucose (10 g/L) minimal medium under aerobic and anaerobic conditions and in LB with glucose (10 g/L) under aerobic conditions. Strains were inoculated in minimal media with 10 g/L glucose or in LB medium with 10 g/L glucose at a starting OD = 0.1–0.15, and they were grown at 37 °C and 250 rpm (New Brunswick I26 incubator shaker) with 1 mM IPTG induction. (*C*) Specific glucose consumption rates of JCL16, NOG21, and NOG26 during production in glucose (10 g/L) minimal medium under anaerobic conditions. (*D*) The extracellular concentration of fermentation products produced within 18 h from JCL16, NOG21, and NOG26 under anaerobic conditions. (*E*) Carbon recovery of JCL16, NOG21, and NOG26 during fermentation. Error bars represent the SD ($n = 3$).

gltA, *acnAB*, *sdhA*, *fumA*, *mdh*, and *pfkB*, by RT-PCR. We found that all of the GS and TCA genes were up-regulated in NOG21 compared with NOG6 (*SI Appendix*, Fig. S3*D*). However, we also found that *tktAB*, *talAB*, and *pfkB* were also up-regulated in NOG21 (*SI Appendix*, Fig. S3*D*). It is possible that other forms of regulation of these genes were altered during evolution.

Potential Beneficial Mutations for the Growth Phenotype of the NOG Strains. In NOG6, part of the synthetic *pck* promoter ($P_L lacO_1$) was deleted (23 bp) (*SI Appendix*, Fig. S2*D*), leading to a decrease in Pck activity (*SI Appendix*, Fig. S1*C*). After this deletion, the gene was likely transcribed from a putative promoter upstream of the sequence (*SI Appendix*, Fig. S2*D*). This result seemed to contradict our design, since the cell relies on this enzyme to convert TCA cycle intermediates to pyruvate. However, we reasoned that if Pck activity is too high, it could drain the TCA cycle intermediates and stop the pathway flux. Thus, there could exist an optimal activity range for Pck activity. This Pck kinetic trap was supported (*SI Appendix*, Fig. S6) by EMRA (24). It seemed that the evolution process was able to adjust the Pck activity to the optimal range.

A point mutation in *pta* (V14F) was also identified in NOG6, which was not present in PHL13. To examine the effect of this mutation, we measured the specific activity of Pta in crude extracts. PHL13 had 43% higher Pta activity than the wild-type *E. coli* (*SI Appendix*, Fig. S1*D*), but the Pta activity was decreased (*SI Appendix*, Fig. S1*D*) due to the V14F mutation evolved from PHL13 to NOG6. *E. coli pta* is positively regulated by the CreBC two-component system (26), which is, in turn, repressed by NagC (27). However, the increased cAMP concentration in PHL13 (*SI Appendix*, Fig. S3 *B* and *C*) stabilized the repression complex for the *nag* operon (28), leading to lower *nagC* expression, up-regulated *creBC*, and finally, the up-regulated *pta*. The increased Pta may cause an imbalance between GS, TCA, and gluconeogenesis flux, as the increased acetyl-CoA concentration may drain the OAA pool in the TCA cycle and decrease the flux through Pck. This effect is supported by EMRA (*SI Appendix*, Fig. S6). Therefore, the mutation in *pta* may compensate for the increased transcription and avoid the flux imbalance. Moreover, we found a genome deletion between 1,747,769 and 1,773,895 (based on the genome sequence of *E. coli* MG1655 genome, NC_000913.2), resulting in the loss of *pyruvate kinase F*, one of the pyruvate kinase genes. This deletion may facilitate the flux in the gluconeogenesis direction to 3-phosphoglycerate. The potential beneficial mutations for the growth phenotype of the NOG strain are summarized in *SI Appendix*, Table S8. Other potential effects of mutations are discussed in *SI Appendix*.

NOG Verification Using ^{13}C Tracing. To validate the pathways used in NOG21, we used 3,4-^{13}C–labeled glucose as a tracer to distinguish between EMP and NOG. If EMP is used, 3,4-labeled glucose will result in labeled formate but unlabeled acetate (Fig. 5*A*). However, if NOG is used, 3,4-labeled glucose will yield unlabeled, single-labeled, and double-labeled acetate (Fig. 5*B*), while formate will be mostly unlabeled. Results (Fig. 5*C*) indeed showed that the wild-type strain JCL16 produced labeled formate (m + 1 ions), while NOG21 only produced unlabeled formate. The mass spectra of pure ^{13}C-labeled and unlabeled formate (*SI Appendix*, Fig. S5) confirmed that 30 and 47 *m/z* ions only came from the labeled formate. These results confirmed that NOG21 does not use the EMP pathway. Also as predicted, acetate produced from JCL16 was unlabeled, while NOG21 produced both m + 1 (10%) and m + 2 ions (19%) (Fig. 5*D*). The double-labeled acetate can only be produced if the full NOG cycle was active. The carbon recovery rates (*SI Appendix*, Table S5) were about 96% and 97% for NOG21 and JCL16, respectively.

Fermentation Profiles of the NOG Strains. To examine the fermentation profiles, NOG21 and NOG26 were precultured aerobically

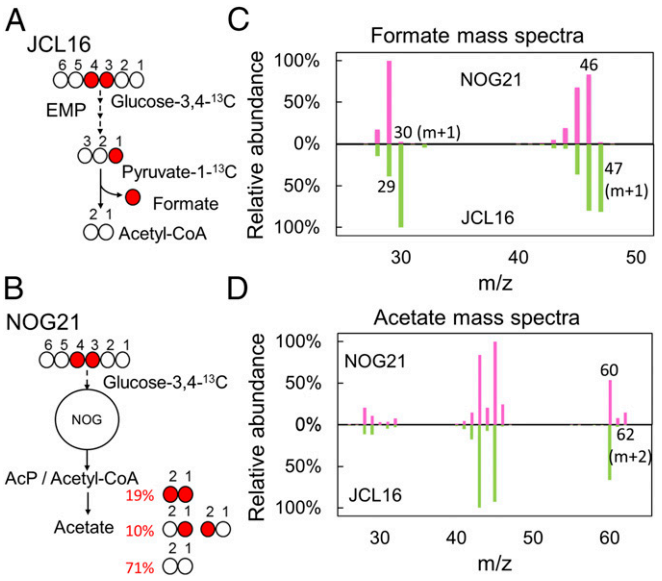

Fig. 5. ^{13}C tracing from glucose-3,4-^{13}C to acetate and formate using JCL16 and NOG21. The labeling pattern of acetate and formate using the (*A*) EMP and (*B*) NOG pathways. The mass spectra of (*C*) formate and (*D*) acetate produced under anaerobic conditions using NOG21 (pink) and JCL16 (green). All spectra were normalized to the most abundant internal peak.

to the stationary phase and concentrated to OD_{600} = 20–25 in fresh glucose minimal medium under anaerobic conditions. This practice mimics some industrial yeast ethanol production processes: growth under aerobic conditions and anaerobic production using concentrated cells. Under this condition, JCL16 produced lactate as the major fermentation product (Figs. 4*D* and 6*A*), while both NOG21 and NOG26 produced acetate as the main product (Figs. 4*D* and 6 *B* and *C*). Additionally, the NOG strains produced acetate almost exclusively after 4 h.

Importantly, these NOG strains produced acetyl-CoA–derived products at yields exceeding the theoretical EMP maximum (67%) (Fig. 4*E*). NOG21 converted 83% of glucose carbon to acetate under anaerobic conditions (Fig. 4*E*). Moreover, NOG21 and NOG26 consumed glucose at the same magnitude during anaerobic fermentation as the wild type (Fig. 4*C*), showing the feasibility of using this strain as a production host.

Although NOG26 had a better growth phenotype than NOG21, it produced more lactate and succinate (Fig. 4*E*), resulting in a lower molar acetate yield. It seems that further evolution from NOG21 to NOG26 likely improved the pathway from acetyl-CoA to pyruvate through GS, leading to additional lactate and succinate production.

Discussion

This work combines rational engineering and directed strain evolution to construct an *E. coli* strain that does not use EMP but is instead dependent on NOG for sugar catabolism. Interestingly, some of the engineering efforts were modified through evolution. For example, the expression levels of Xpk and Pck were reduced through evolution, presumably to avoid "kinetic traps" caused by flux imbalance. In addition, many regulatory circuits were altered to adapt to the grossly rewired biochemical infrastructure. Such fine-tuning of regulation would be difficult to design a priori. The coupling of growth with NOG enabled the cell to adapt its metabolic and regulatory circuits to this metabolic strategy through directed evolution. While the NOG strain produced an acetyl-CoA–derived product at yields exceeding the theoretical EMP maximum, the product distribution may need to be further optimized. For example, the increased production of succinate and lactate by NOG26 may be eliminated by rational engineering to optimize the desired product.

To fully realize the potential of NOG, an NOG strain must be capable of making compounds more reduced than acetate. To do so, one must generate reducing equivalents from the carbon source or provide them externally. Generating reducing equivalents from the carbon source leads to CO_2 emission and reduction of carbon yield, while providing external reducing equivalents incurs additional cost. It is the competition between these two costs that determines the economic benefit of the NOG strain.

External reducing equivalents can be provided by renewable H_2 or formic acid. For example, one can produce 3 mol of ethanol from 1 mol of glucose using NOG through reductive fermentation:

$$C_6H_{12}O_6 + 6\ H_2 + ATP \rightarrow 3\ C_2H_5OH + 3\ H_2O,$$

which represents a 50% increase of carbon yield compared with the EMP-based fermentation. To produce the same amount of ethanol using native EMP would require 1.5 mol of glucose:

$$1.5\ C_6H_{12}O_6 \rightarrow 3\ C_2H_5 + 3\ CO_2.$$

Thus, the NOG process is more carbon efficient but requires 6 mol of H_2 and 1 mol of ATP to save 0.5 mol of glucose. Assuming that the phosphate/oxygen ratio is 2.5 means that 2.5 mol of ATP can be produced from the movement of 2 mol electrons (1 mol of H_2) through a defined electron transport chain. Thus, the NOG process requires 6.4 mol of H_2 total to

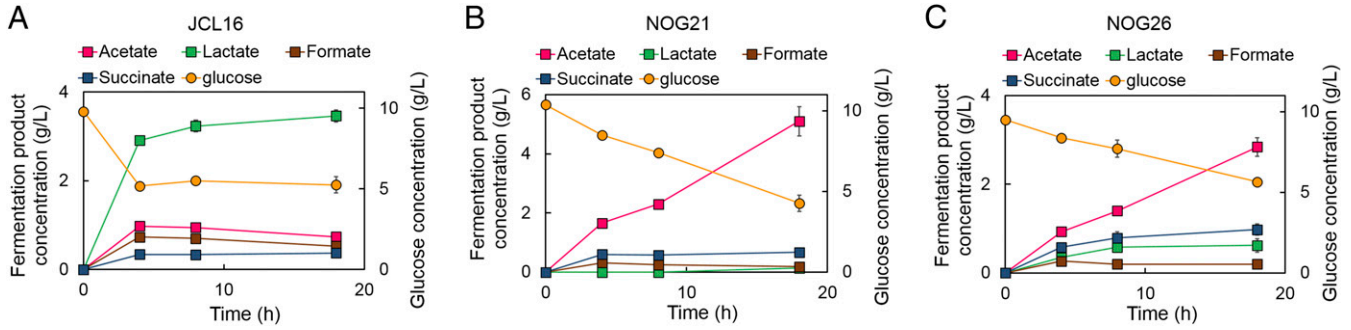

Fig. 6. Fermentation in glucose minimal medium using packed cell production. Glucose and fermentation product concentrations during the anaerobic production in glucose minimal medium using (*A*) JCL16, (*B*) NOG21, and (*C*) NOG26 at 37 °C. Strains were precultured in LB medium with 10 g/L glucose and 1 mM IPTG aerobically at 37 °C and 250 rpm for 16 h. Then, cells were concentrated to OD_{600} = 25–30 in glucose (10 g/L) minimal medium anaerobically at 37 °C and 250 rpm (New Brunswick I26 incubator shaker). Error bars represent the SD (n = 3).

save 0.5 mol of glucose. If the glucose price is \$0.4/kg, it would require H_2 cost to be less than \$2.81/kg to be economically competitive compared with EMP-based metabolism. With the fast progress of renewable electricity and water electrolysis, an economical NOG-based process is realistic.

The NOG-based reductive fermentation described above essentially fixes CO_2 with H_2 (or formate or other reducing agents) together with sugar fermentation. To achieve the reductive fermentation, one must express hydrogenase or formate dehydrogenase in the NOG strain to allow the input of additional reducing equivalents. Although native acetogens can produce acetate from H_2 and CO_2 using an energy-efficient but oxygen-sensitive Wood–Ljungdahl pathway (29, 30), the plethora of genetic tools available to *E. coli* and the vast experience gained from its industrial applications provide incentives for further exploration of the NOG-based *E. coli*. Interestingly, NOG has not been adopted in nature as the sole path for carbohydrate catabolism, although many organisms have all of the required enzymes (31–34). This leads to the possibility that generating reducing equivalents and fast growth are more important than carbon conservation in naturally evolved organisms.

There are multiple mutations accumulated in the evolution of the NOG strains. The minimal set of the mutations that are responsible for the observed phenotypes remains to be determined. In summary, the NOG-dependent *E. coli* strains presented here may provide a rich opportunity for physiological characterizations as well as potential practical applications.

Materials and Methods

Details and a full list of abbreviations are in *SI Appendix*.

Bacterial Strains and Plasmids. Strains and plasmids used in this study are listed in *SI Appendix*, Tables S6 and S7.

Chemicals and Reagents. All chemicals unless otherwise specified were acquired from Sigma-Aldrich or Thermo Fisher Scientific. Phire Hot Start II DNA polymerase, DpnI, and Gibson Assembly Master Mix were purchased from New England Biolabs. Glucose-3,4-^{13}C was purchased from Omicron Biochemicals.

Medium and Cultivation. Details are provided in *SI Appendix*.

Genomic Manipulation. Details are provided in *SI Appendix*.

Individual Enzyme Assays. Details are provided in *SI Appendix*.

Whole-Pathway Assay. *E. coli* strains were grown in glucose minimal media supplemented with acetate and lysed by BugBuster (Sigma-Aldrich). Protein concentration was measured by Bradford assay. The assay mixture contains phosphate buffer (pH 7.5), 5 mM $MgCl_2$, 1 mM thiamine pyrophosphate, and 10 mM F6P; 40 μg of cell crude extract was added to the assay mixture with purified enzymes (at least 5 μg each) for 2.5 h at room temperature. Then, the AcP concentration was measured by the colorimetric assay as described before (7).

RT-PCR. Details are provided in *SI Appendix*.

Genome Sequence. Details are provided in *SI Appendix*.

NOG Strain Evolution. Details are provided in *SI Appendix*.

Tkt and Tal Bioprospecting. Details are provided in *SI Appendix*.

EMRA. Details are provided in *SI Appendix*.

Growth Characterization. Details are provided in *SI Appendix*.

^{13}C Tracing and Fermentation Test. Strains were grown in LB medium with glucose (10 g/L) aerobically with 1 mM isopropyl β-D-1-thiogalactopyranoside (IPTG) induction for 16 h. Then, the cells were washed once and concentrated in the production medium at OD_{600} = 20–25 anaerobically. Labeled glucose was used for the ^{13}C tracing experiment. Concentrated cells were incubated at 37 °C on a rotary shaker (250 rpm) anaerobically. Samples were collected anaerobically.

Analytical Methods. Individual assays were measured spectrophotometrically using an Agilent 8453 UV-Vis spectrophotometer (Agilent Technologies). Organic acids were measured by HPLC (Agilent Technologies and Thermo Fisher Scientific). Labeled acetate and formate were analyzed by GC-MS (Agilent Technologies). Details are provided in *SI Appendix*.

ACKNOWLEDGMENTS. We thank Mei-yeh Lu and the High Throughput Sequencing Core at the Biodiversity Research Center in Academia Sinica for performing the next-generation sequencing experiments. We thank Ranuka T. Hewage and Hsiao-Ching Lin (Academia Sinica) for determining the purity of ^{13}C-labeled glucose. We thank Igor W. Bogorad and Chang-Ting Chen of the laboratory of J.C.L. for useful scientific discussions. We also thank Sawako Konishi, Siyi Fiona Guo, Hao Yuan, Kushal Nimkar, Justin Kahng, Maria Chun, and Joanna Marshall of the laboratory of J.C.L. for their technical support in enzyme assays and strain evolution. *M. buryatense* 5GB1 was a gift from Mary Lidstrom (University of Washington). This work was supported, in part, by US Department of Energy Grants DE-SC0012384 and DE-SC0006698.

1. Clomburg JM, Gonzalez R (2010) Biofuel production in Escherichia coli: The role of metabolic engineering and synthetic biology. *Appl Microbiol Biotechnol* 86:419–434.
2. Felnagle EA, Chaubey A, Noey EL, Houk KN, Liao JC (2012) Engineering synthetic recursive pathways to generate non-natural small molecules. *Nat Chem Biol* 8: 518–526.
3. Pokusaeva K, Fitzgerald GF, van Sinderen D (2011) Carbohydrate metabolism in *Bifidobacteria*. *Genes Nutr* 6:285–306.
4. Kocharin K, Siewers V, Nielsen J (2013) Improved polyhydroxybutyrate production by *Saccharomyces cerevisiae* through the use of the phosphoketolase pathway. *Biotechnol Bioeng* 110:2216–2224.
5. de Jong BW, Shi S, Siewers V, Nielsen J (2014) Improved production of fatty acid ethyl esters in *Saccharomyces cerevisiae* through up-regulation of the ethanol degradation pathway and expression of the heterologous phosphoketolase pathway. *Microb Cell Fact* 13:39.
6. Chinen A, Kozlov YI, Hara Y, Izui H, Yasueda H (2007) Innovative metabolic pathway design for efficient l-glutamate production by suppressing CO_2 emission. *J Biosci Bioeng* 103:262–269.
7. Bogorad IW, Lin T-S, Liao JC (2013) Synthetic non-oxidative glycolysis enables complete carbon conservation. *Nature* 502:693–697.
8. Schaaper RM (1988) Mechanisms of mutagenesis in the *Escherichia coli* mutator *mutD5*: Role of DNA mismatch repair. *Proc Natl Acad Sci USA* 85:8126–8130.
9. Seta FD, Boschi-Muller S, Vignais ML, Branlant G (1997) Characterization of *Escherichia coli* strains with *gapA* and *gapB* genes deleted. *J Bacteriol* 179:5218–5221.
10. Nakahigashi K, et al. (2009) Systematic phenome analysis of *Escherichia coli* multiple-knockout mutants reveals hidden reactions in central carbon metabolism. *Mol Syst Biol* 5:306.
11. Grabar TB, Zhou S, Shanmugam KT, Yomano LP, Ingram LO (2006) Methylglyoxal bypass identified as source of chiral contamination in l(+) and d(-)-lactate fermentations by recombinant *Escherichia coli*. *Biotechnol Lett* 28:1527–1535.
12. Boschi-Muller S, Azza S, Pollastro D, Corbier C, Branlant G (1997) Comparative enzymatic properties of GapB-encoded erythrose-4-phosphate dehydrogenase of *Escherichia coli* and phosphorylating glyceraldehyde-3-phosphate dehydrogenase. *J Biol Chem* 272:15106–15112.
13. Maloy SR, Nunn WD (1982) Genetic regulation of the glyoxylate shunt in *Escherichia coli* K-12. *J Bacteriol* 149:173–180.
14. Shimada T, Fujita N, Yamamoto K, Ishihama A (2011) Novel roles of cAMP receptor protein (CRP) in regulation of transport and metabolism of carbon sources. *PLoS One* 6:e20081.
15. Nakano M, Ogasawara H, Shimada T, Yamamoto K, Ishihama A (2014) Involvement of cAMP-CRP in transcription activation and repression of the pck gene encoding PEP carboxykinase, the key enzyme of gluconeogenesis. *FEMS Microbiol Lett* 355: 93–99.
16. Kotlarz D, Garreau H, Buc H (1975) Regulation of the amount and of the activity of phosphofructokinases and pyruvate kinases in Escherichia coli. *Biochim Biophys Acta* 381:257–268.
17. Weisser P, Krämer R, Sahm H, Sprenger GA (1995) Functional expression of the glucose transporter of *Zymomonas mobilis* leads to restoration of glucose and fructose uptake in *Escherichia coli* mutants and provides evidence for its facilitator action. *J Bacteriol* 177:3351–3354.
18. Meyer D, Schneider-Fresenius C, Horlacher R, Peist R, Boos W (1997) Molecular characterization of glucokinase from *Escherichia coli* K-12. *J Bacteriol* 179:1298–1306.
19. Babul J, Guixé V (1983) Fructose bisphosphatase from *Escherichia coli*. Purification and characterization. *Arch Biochem Biophys* 225:944–949.
20. Hines JK, Fromm HJ, Honzatko RB (2006) Novel allosteric activation site in *Escherichia coli* fructose-1,6-bisphosphatase. *J Biol Chem* 281:18386–18393.
21. Steinsiek S, Bettenbrock K (2012) Glucose transport in *Escherichia coli* mutant strains with defects in sugar transport systems. *J Bacteriol* 194:5897–5908.

22. Quail MA, Guest JR (1995) Purification, characterization and mode of action of PdhR, the transcriptional repressor of the pdhR-aceEF-lpd operon of Escherichia coli. *Mol Microbiol* 15:519–529.
23. Zhang Z, et al. (2005) Functional interactions between the carbon and iron utilization regulators, Crp and Fur, in *Escherichia coli*. *J Bacteriol* 187:980–990.
24. Lee Y, Lafontaine Rivera JG, Liao JC (2014) Ensemble Modeling for robustness analysis in engineering non-native metabolic pathways. *Metab Eng* 25:63–71.
25. Dong T, Schellhorn HE (2009) Control of RpoS in global gene expression of *Escherichia coli* in minimal media. *Mol Genet Genomics* 281:19–33.
26. Avison MB, Horton RE, Walsh TR, Bennett PM (2001) *Escherichia coli* CreBC is a global regulator of gene expression that responds to growth in minimal media. *J Biol Chem* 276:26955–26961.
27. Oberto J (2010) FITBAR: A web tool for the robust prediction of prokaryotic regulons. *BMC Bioinformatics* 11:554.
28. Plumbridge J, Kolb A (1995) Nag repressor-operator interactions: Protein-DNA contacts cover more than two turns of the DNA helix. *J Mol Biol* 249:890–902.
29. Tracy BP, Jones SW, Fast AG, Indurthi DC, Papoutsakis ET (2012) *Clostridia*: The importance of their exceptional substrate and metabolite diversity for biofuel and biorefinery applications. *Curr Opin Biotechnol* 23:364–381.
30. Fast AG, Papoutsakis ET (2012) Stoichiometric and energetic analyses of non-photosynthetic CO_2-fixation pathways to support synthetic biology strategies for production of fuels and chemicals. *Curr Opin Chem Eng* 1:380–395.
31. Schramm M, Klybas V, Racker E (1958) Phosphorolytic cleavage of fructose-6-phosphate by fructose-6-phosphate phosphoketolase from *Acetobacter xylinum*. *J Biol Chem* 233:1283–1288.
32. Fandi KG, Ghazali HM, Yazid AM, Raha AR (2001) Purification and N-terminal amino acid sequence of fructose-6-phosphate phosphoketolase from *Bifidobacterium* longum BB536. *Lett Appl Microbiol* 32:235–239.
33. Meile L, Rohr LM, Geissmann TA, Herensperger M, Teuber M (2001) Characterization of the D-xylulose 5-phosphate/D-fructose 6-phosphate phosphoketolase gene (xfp) from *Bifidobacterium lactis*. *J Bacteriol* 183:2929–2936.
34. Liu L, et al. (2012) Phosphoketolase pathway for xylose catabolism in *Clostridium acetobutylicum* revealed by 13C metabolic flux analysis. *J Bacteriol* 194:5413–5422.